

Extensibility-Enriched Spinnability and Enhanced Sorption and Strength of Centrifugally Spun Polystyrene Fiber Mats

Jorgo Merchiers, Naveen K. Reddy,* and Vivek Sharma*



Cite This: *Macromolecules* 2022, 55, 942–955



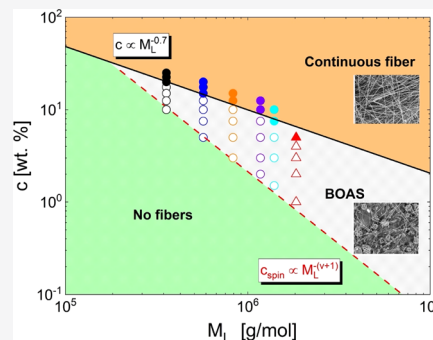
Read Online

ACCESS |

Metrics & More

Article Recommendations

ABSTRACT: We show that incorporating ultrahigh molecular weight (UHM_w) polymer fractions into spinning dopes improves their spinnability and facilitates the centrifugal force spinning (CFS) of polystyrene (PS) fiber mats with enhanced mechanical and sorption properties. For matched polymer concentration, c , and solvent type, the UHM_w additive at a low weight fraction (<0.1) only weakly influences shear viscosity. We attribute the enhanced spinnability and fiber properties to change in extensibility (stretched to equilibrium coil size ratio), quantified using the extensibility-averaged molecular weight, M_L , that accounts for the role of stretched chain hydrodynamics and extensional rheology response. Although many studies argue that spinnable solutions lie above the entanglement concentration on the c – M_w plots, we show that the UHM_w additives facilitate fiber formation below the computed entanglement concentration for extensibility-enriched (EE) polymer solutions. We highlight the role of extensibility and dispersity by locating the minimum spinnable concentration, c_{spin} , and the concentration, c_{BC} , for the transition from beaded to continuous fiber formation on a c – M_L plot. We show that extensibility-enriched solutions display $c_{\text{spin}} \propto M_L^{-b}$ with $b = 1 + \nu$ and $c_{\text{BC}} \propto M_L^{-b}$ with $b = 3\nu - 1$ due to significant strain hardening and large Trouton ratios that delay pinch-off. Additionally, we posit that in low-extensibility solutions, including low M_w or lower flexibility polymers, spinnability benefits from the steep viscosity increase on the solvent loss for volatile entangled (VE) polymer solutions, requiring $c_{\text{spin}} \propto c_e \propto M_w^{-b}$ with $b = 1 + \nu$, explaining why entanglements promote fiber formation.



INTRODUCTION

Inventing and optimizing spinning techniques for high throughput, cost-efficient production of fibers from both commercial and novel polymers has driven extensive academic and industrial research for over a century.^{1–7} Many applications in tissue engineering and healthcare, environmental safety and remediation, energy storage and production, and separations require nonwoven fiber meshes or membranes that simultaneously satisfy multiple design needs and functionalities, including ultrahigh surface-to-volume ratio, suitable permeability, mechanical and chemical stability, and appropriate wettability.^{3–14} Despite significant progress in making nonwovens with electrospinning (ES), challenges with scalability, the need for a high voltage source, limited solvent choices, and low production rates are driving the search for viable alternatives.^{4–7,12–15} Here, we focus on addressing the spinnability challenge using an alternative method called centrifugal force spinning (CFS). Although similar methods were first patented over a century back and then used to make cotton candy and glass wool, intense activity to make polymeric fibers using this technique began a decade back under many names: centrifugal spinning, force spinning, rotary spinning, or rotary jet spinning.^{4–8,14–27} In contrast with melt-CFS used for making cotton candy or glass wool from viscous fluids and/or reactive CFS that uses monomer-based spinning

dope,^{20,21} we focus on solution-CFS that requires the processing of rheologically complex polymer solutions. Furthermore, fiber formation involves evaporative loss of the solvent leading to significant viscosity increase before solidification. Therefore, CFS shares the rheology–structure properties quests of fiber spinning methods like dry spinning and electrospinning, including the practical and theoretical challenges in correlating spinnability to the rheological response as influenced by the choice of polymer concentration, molecular weight, dispersity, and solvent properties.^{1–5,14,26–40} Finding universal features in terms of the influence of the polymer (c , M_w , and physicochemical properties) and solvent for controlling fiber properties and the morphology remain critical technological and scientific problems.^{1–5,24–34,39–50} Here, we investigate the influence of a polymer concentration, molecular weight, and dispersity on centrifugally spun fiber

Received: October 17, 2021

Revised: December 4, 2021

Published: January 24, 2022



morphology, sorption, and mechanical properties for matched solvent and processing conditions.

Describing the spinnability of polymer solutions involves several challenging problems: a complex interplay of nonlinear shear and extensional rheological response, free surface flows and instabilities, and evaporative mass loss and cooling from mobile jets.^{1–4,23–30,50–54} For example, Petrie^{28,29} provides both historical perspectives and describes the many long-standing challenges faced in correlating spinnability to the shear and extensional rheology response. Many studies attribute spinnability to the influence of entanglements or topological constraints^{10,17,31–33,46,48–50} that arise in solutions (and melts) above the entanglement concentration, c_e (and beyond entanglement molecular weight, M_e), and hence the spinnability diagrams are presented with molecular weight, M_w , and concentration, c , as the coordinates. However, a few reports show that adding a small fraction of ultrahigh molecular weight (UHM_w) facilitates fiber formation from unentangled polymer solutions.^{39–41} For instance, Yu et al.³⁹ demonstrated that electrospinning from unentangled PEO solutions results in fibers on addition of a small amount of the UHM_w component. Even though spinning dopes displayed similar values of rate-independent shear viscosity, Yu et al. argued that spinnability correlates with an increase in elasticity and extensional viscosity, as observed in their capillary breakup extensional rheometer (CaBER) measurements.³⁹

In both ES and CFS, the strong flows associated with stretching and thinning liquid jets stretch and align polymers stretching long enough time-of-flight, t_{flight} , and evaporation time, t_{evap} . However, increasing t_{flight} or t_{evap} is detrimental if either exceeds the time needed for the capillarity-driven growth of sinusoidal perturbations that create beads-on-a-string (BOAS) or beaded fibers and, possibly, just drops (or beads, after drying). Processability maps based on zero-shear viscosity, η_0 , and surface tension, σ , can be drawn using the viscocapillary time, $t_{\text{vc}} = \eta_0 D_0 / \sigma$, to capture the role of the interplay of viscous stress and capillarity. Equivalent maps use Ohnesorge number, $Oh = \eta_0 / \sqrt{\rho \sigma D_0}$, which is the dimensionless measure of viscous effects obtained by scaling t_{vc} with an inertiocapillary time, $t_{\text{ic}} = \sqrt{\rho R_0^3 / \sigma}$, plotted against a Capillary number, $Ca = t_{\text{vc}} / t_{\text{cent}}$ such that $t_{\text{cent}} = R_0 / U_{\text{cent}}$ depends on the centrifugal speed.²⁵ As free surface flows associated with fiber formation invariably involve nonlinear deformation and streamwise velocity gradients associated with extensional rheology response, the utility of such Oh – Ca or the c – M_w processability maps is limited by the inadequate accounting for the influence of elasticity and rate- or concentration-dependent extensional rheology response that is not linearly correlated with the corresponding shear rheology response.^{50,55–71}

Without direct measurements of extensional rheology response, Palangetic et al.⁴⁰ argued that the minimum spinnable concentration, c_{spin} , must depend on enhancement in extensional viscosity on addition of an ultrahigh molecular weight fraction, and hence, they defined an extensibility-averaged molecular weight, M_L . The zero-shear viscosity of dilute solutions depends on the unperturbed coil size, $\langle R^2 \rangle^{1/2} \propto M^\nu$. Here, the exponent, ν , that depends on the polymer–solvent interactions is often called the solvent quality parameter. In contrast, the steady, terminal extensional viscosity, η_E^∞ , in the FENE-P model is directly proportional to the square of the extensibility, $\eta_E^\infty \propto L_E^2$. The parameter extensibility, L_E , represents the ratio of the maximally stretched

state of the polymer, R_{max} , to its root mean square equilibrium coil size, R_0 , and $L_E \equiv N_K^{1-\nu}$, with the number of Kuhn segments determined using $N_K = M/M_0$ and using the Kuhn monomer weight (for PS, $M_0 = 0.72 \text{ kg}\cdot\text{mol}^{-1}$). Palangetic et al.⁴⁰ showed that the critical spinnability concentration computed using $c_{\text{spin}} \sim M_L^{(\nu+1)} \sim M_L^{1.566}$ matches with the experimentally determined c_{spin} for many electrospun polymer–solvent combinations, though they directly illustrated the dispersity effect only for poly(methyl methacrylate) fibers. We posit that a similar criterion for minimum spinnable concentration, c_{spin} , should be applicable for the centrifugal force spinning of polymer solutions and, hence, could be influenced by the inclusion of a small amount of ultrahigh molecular weight or UHM_w component, motivating this study.

The manuscript is organized as follows. We investigate the influence of molecular weight and dispersity on spinnability by centrifugal force spinning polystyrene (PS) fibers from bidisperse solutions prepared by incorporating a relatively small weight fraction ($w_U < 0.1$) of PS = 2000 kg·mol^{−1} as the UHM_w additive. We picked polystyrene (PS) to investigate the interplay between spinnability, polymer physics, rheology, and processing to benefit from the complementary studies, especially involving electrospinning.^{35–37,42,48,72–76} Furthermore, PS fiber mats offer promising candidates for oil sorption, significantly for tackling maritime oil pollution, while simultaneously recycling this commodity plastic.^{77–82} We show that the change in zero-shear viscosity, η_0 , of bidisperse solutions follows a single universal curve on plotting against scaled concentrations or the Berry number, $c[\eta]$, that computes the degree of overlap expressed as the product of concentration and intrinsic viscosity. We characterize the morphology, sorption, and mechanical properties of the centrifugally spun fiber mats as a function of the UHM_w fraction. We show that spinnability and morphology changes are correlated with the extensibility-averaged molecular weight, M_L . In addition to exploring if the c_{spin} – M_L relationship outlined for minimal spinnable concentration in ES applies for CFS, we posit that the beaded-to-continuous filament (BC) transition should depend on the hydrodynamics of stretched chains, extensibility, and extensional rheology response. We seek to define and identify this transition concentration, c_{BC} , as the locus of points beyond which continuous fibers appear. Here, we develop a spinnability map as influenced by the choice of the polymer, with associated macromolecular parameters, including extensibility, molecular weight, and dispersity, assuming matched solvent properties and processing conditions. We anticipate that our study will inspire the use of extensibility and dispersity as tunable parameters to spin fibrous materials with suitable morphology and physicochemical properties.

■ MATERIALS AND METHODS

Matrix, Ultrahigh, and Bidisperse Polystyrene (PS) Solutions. The solvent, tetrahydrofuran (THF), and polymers purchased from VWR Chemicals (Oud-Heverlee, Belgium) were used without further purification. Bidisperse blends with increasing molecular weight and dispersity were prepared using a matrix (M) with supplier-listed weight-averaged molecular weight, $M_{\text{wM}} = 280 \text{ kg}\cdot\text{mol}^{-1}$, and the UHM_w component with $M_{\text{wU}} = 2000 \text{ kg}\cdot\text{mol}^{-1}$ with $w_U < 0.1$. Additional datasets obtained for PS of $M_w = 190 \text{ kg}\cdot\text{mol}^{-1}$ are included for completeness.⁴⁸

The number and weight-averaged molecular weight, M_n and M_w , and dispersity, $\mathbb{D} = M_w/M_n$, were determined via size-exclusion chromatography (SEC). We used a Tosoh EcoSEC HLC-8320GPC,

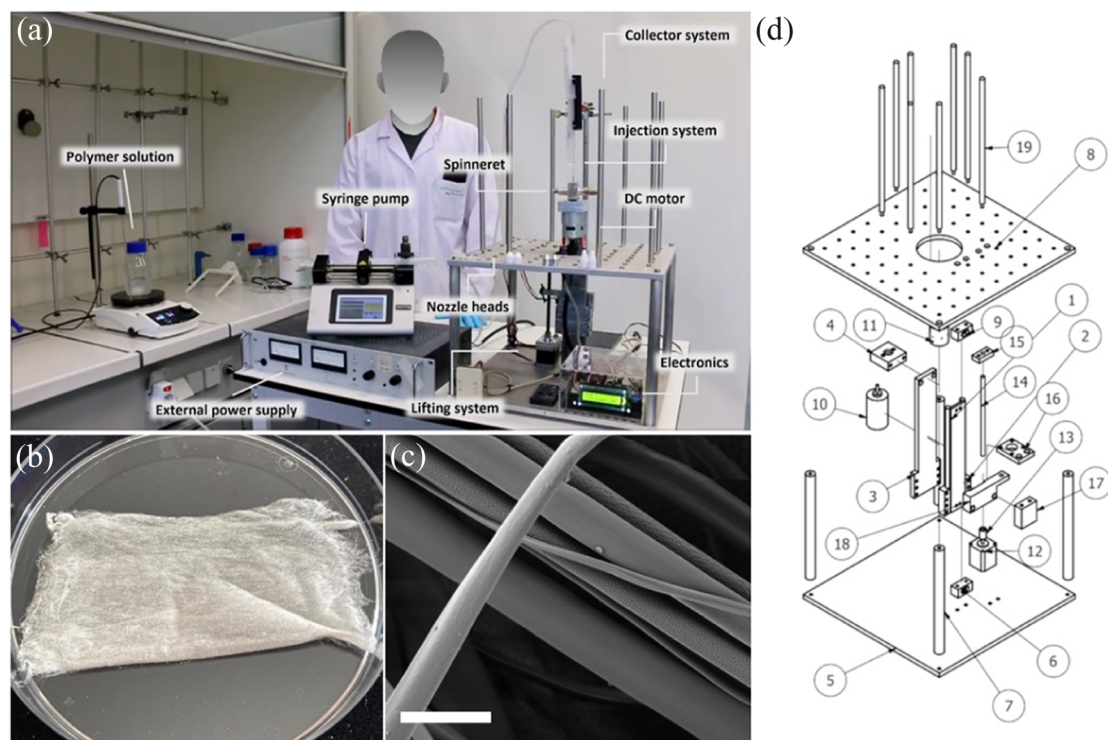


Figure 1. Centrifugal force spinning (CFS) apparatus used for preparing PS fiber mats. (a) Labeled photograph of the centrifugal force spinning apparatus, including an injector, a spinneret, a DC motor, and the electronics that allow control over the rotational speed. (b) Image showing an example of a fiber mat formed with the collected fibers. (c) SEM image showing that the highly aligned fibers have nanoscopic pores. The scale bar is $4\ \mu\text{m}$. (d) Exploded view of the setup showing the following parts—1: guide rail, 2: motor guide, 3: motor holder, 4: motor holder top, 5: bottom plate, 6: guide rail holder bottom, 7: standoffs (4), 8: top plate, 9: guide rail holder top, 10: DC motor, 11: cup, 12: lid, 13: stepper motor, 14: threaded rod sleeve, 15: threaded rod, 16: threaded rod holder, 17: stepper motor holder top, 18: stepper motor holder bottom, 19: lifting arm, and 20: collection posts.

comprising an autosampler, a PSS guard column SDV ($50 \times 7.5\ \text{mm}$), followed by $2 \times$ PLgel Mixed-C columns ($5\ \mu\text{m}$, $300\ \text{mm} \times 7.5\ \text{mm}$), and a differential refractive index detector (Tosoh EcoSEC RI) that employs high-performance liquid chromatography (HPLC)-grade THF as the eluent at $40\ ^\circ\text{C}$ with a flow rate of $1\ \text{mL}\cdot\text{min}^{-1}$. Toluene was used as the flow marker. The SEC system was calibrated using linear, low-dispersity polystyrene (PS) standards from PSS Laboratories ranging from 390 to $3.69 \times 10^6\ \text{g}\cdot\text{mol}^{-1}$ using the corresponding Mark–Houwink–Sakurada parameters for PS: $K = 14.1 \times 10^{-5}\ \text{dL}\cdot\text{g}^{-1}$ and $a = 0.70$. The solution was filtered over a $0.45\ \mu\text{m}$ filter and injected into the SEC column.

Shear Viscosity of the Spinning Dope. The zero-shear viscosity of all of the solutions was determined with an ARG-2 stress-controlled rheometer (TA Instruments, New Castle, DE) using the cone-and-plate geometry ($40\ \text{mm}$ diameter, $54\ \mu\text{m}$ gap, 1° cone angle). A Peltier element was used for a fixed temperature of $25\ ^\circ\text{C}$, and a solvent trap avoided evaporative loss during the measurements. Steady-state viscosity was measured at constant values for shear rates, ranging from 0.1 to $1000\ \text{s}^{-1}$, with a tolerance of 3%.

Centrifugal Force Spinning of PS Fibers Using a Specially Designed Setup. We designed and built the bespoke centrifugal force spinning (CFS) setup shown in the labeled photograph in Figure 1a. The photographed CFS setup in Figure 1a produces dense, centrifugally spun PS fiber mats with a high degree of filament alignment (see Figure 1b, for example), and the scanning electron microscopy (SEM) images show that the fibers are porous with pores $< 100\ \text{nm}$ in size (Figure 1c). The diagram included in Figure 1d shows the parts listed in the figure caption required for emulating the setup. The carefully designed injector system has a syringe pump to feed an arm-style spinneret with two nozzles symmetrically mounted on a variable RPM (rotations per minute) motor. Likewise, the collector assembly is equipped to shift pillars and liftable base to adjust the collector–nozzle distance. The influence of nozzle type and

materials, rotational speeds, and solvent composition on the fiber morphology was explored in our previous contributions.^{48–50} An environmental chamber could be added in future to control temperature, humidity, and air flow.

Characterization of Diameter, Tensile Properties, and Sorption Behavior of Fiber Mats. The morphology of PS fibers was visualized using a $15\ \text{kV}$ Hitachi TM3000 tabletop scanning electron microscope (SEM) (Hitachi, Tokyo, Japan) with a $5\ \text{mm}$ working distance. The analysis of at least three SEM images was carried out using ImageJ software (Bethesda, MD) to measure the diameter of at least 100 fibers, selected at random to obtain a statistically representative measurement. Tensile testing experiments of centrifugally spun fiber mats with dimensions of $60\ \text{mm} \times 10\ \text{mm}$ were carried out on a Tinius Olsen (SST) apparatus (Redhill, U.K.), with a tensile speed of $1\ \text{mm}\cdot\text{min}^{-1}$ and a preload of $0.5\ \text{N}$. The fiber mats were collected and analyzed in an aligned orientation, without stretching by mounting into the clamps with a length of $20\ \text{mm}$. The cross-sectional area, $A = V/l$, of samples is determined using volume, V , computed from density, $\rho = m/V$ (for PS = $1.00\ \text{g}\cdot\text{cm}^{-3}$), mass, m , and length, l . Oil sorption tests were carried out on the spun fiber samples that were dried for at least 4 days at room temperature after spinning experiments. Artificial oil–water baths were prepared by adding $10\ \text{mL}$ of the chosen oil on top of $20\ \text{mL}$ of H_2O into a $100\ \text{mL}$ beaker. Approximately $0.1\ \text{g}$ of as-spun fibrous sorbents were left in the oil–water baths for $60\ \text{min}$. After sorption, the samples were pulled out and drained for $60\ \text{s}$ before weighing. After that, sorption capacity, $Q = (m_s - m_0)/m_0$, was measured for three oils in terms of the relative mass increase (g/g) using the difference between the final soaked mass, m_s , and the initial dry mass, m_0 , respectively.

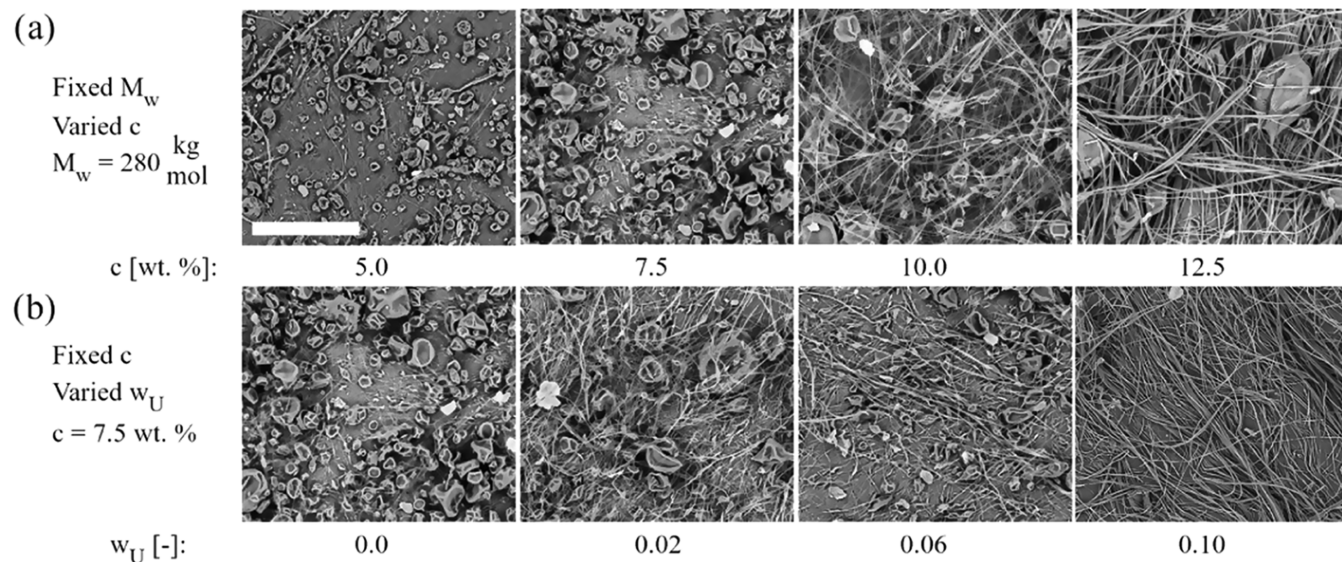


Figure 2. Influence of the ultrahigh molecular weight additive on spinnability. (a) SEM images show increasing polymer concentration from $c = 5$ to 12.5 wt % for PS280 leading to a transition from beads to beaded to continuous fibers. (b) Adding the UHM_w component in low weight fraction $w_U < 0.1$ in the spinning dope improves spinnability and impacts the fiber morphology. The scale bar is 100 μm .

RESULTS

The fibers described in this study were centrifugally spun from PS solutions in THF as a solvent using matched processing conditions: rotational speed (4000 rpm), collector distance (12 cm), and nozzle diameter (0.6 mm) under similar laboratory conditions. SEM images in Figure 2a show changes in the morphology from beads only for $c = 5$ and 7.5 wt % to beaded fibers or beads-on-a-string (BOAS) structures at $c = 10$ wt % for matched environmental and processing conditions. Continuous fibers form for the polymer concentration, $c = 12.5$ wt % PS280. Figure 2b shows that the low weight fraction, $w_U < 0.1$, of the ultrahigh molecular weight (UHM_w) additive facilitates fiber formation even for $c = 7.5$ wt %.

We characterized the molecular weight distribution (MWD) of the as-received polymers and their mixtures using SEC, as shown in Figure 3. We calculated the number, weight, and viscosity-averaged molecular weights listed in Table 1 as M_n ,

Table 1. Summary of GPC Results including Different Moments of Molecular Weight [$\text{kg}\cdot\text{mol}^{-1}$]^a

w_U	M_n	M_w	M_v	M_L	\mathcal{D}	η_0
0	106	271	243	571	2.6	0.032
.02	105	305	267	830	2.9	0.036
.06	107	365	308	1174	3.4	0.046
.10	112	433	358	1397	3.9	0.073
1	1217	1581	1543	1843	1.3	

^aThe viscosity values [$\text{Pa}\cdot\text{s}$] are measured for PS solutions with $c = 10$ wt %.

M_w , and M_v , respectively. Additionally, we computed the extensibility-averaged molecular weight, M_L , using the following equation

$$M_L = \left(\frac{\sum_i N_i M_i^{2+\nu}}{\sum_i N_i M_i} \right)^{1/(\nu+1)} = \left(\sum_i w_i M_i^{1+\nu} \right)^{1/(\nu+1)} \quad (1)$$

Equation 1 was introduced by Palangetic et al.⁴⁰ to account for the influence of stretched chain hydrodynamics that

determines the extensional rheology response. Here, ν is the solvent quality parameter, M_i is the molecular weight for a species of length i , $w_i = N_i M_i / \sum_i N_i M_i$ is the weight fraction of species i , and $N = \sum_i N_i$ is the total number of chains. The SEC analysis of the MWD for UHM_w (PS2000) and matrix (PS280) samples, included in Figure 3a, yields values $M_{wU} = 1581 \text{ kg}\cdot\text{mol}^{-1}$ and $M_{wM} = 270.7 \text{ kg}\cdot\text{mol}^{-1}$, respectively, that are lower than quoted by the supplier. In contrast, the dispersity, $\mathcal{D}_U = 1.3$, agrees with the supplier's value. The SEC traces in Figure 3a show that PS280 has hardly any UHM_w polymer chains.

Bidisperse systems formulated using weight fractions, $w_U = 0.02, 0.06, \text{ and } 0.1$, for the sake of exploring the influence of the UHM_w additive on spinnability show a second peak due to the UHM_w fraction (PS2000). Figure 3a also includes SEC data for an additional sample with the supplier-quoted $M_w = 190 \text{ kg}\cdot\text{mol}^{-1}$. Increasing the weight fraction of the UHM_w component (PS2000) exercises a more substantial influence on M_L as the difference in contour length of PS280 and PS2000 chains is greater than the difference in their equilibrium coil size. Hereafter, we refer to solutions containing UHM_w fraction as extensibility-enriched polymer solutions. Figure 3b shows the plotted data for M_L and M_w as a function of dispersity, \mathcal{D} . The values range between $M_L = 571 \text{ kg}\cdot\text{mol}^{-1}$ for the matrix polymer (PS280) and $M_L = 1843 \text{ kg}\cdot\text{mol}^{-1}$ for the ultrahigh polymer (PS2000), and the difference between M_L and M_w is larger for PS280 ($\mathcal{D}_M = 2.55$) than for PS2000 ($\mathcal{D}_U = 1.30$). As the UHM_w weight fraction increases, M_L shows a more pronounced increase than M_w . Table 1 lists the average values computed using GPC or SEC (though M_L for the bidisperse system can also be estimated) and also includes the zero-shear viscosity values for $c = 10$ wt %, and even for the extensibility-enriched (EE) polymer solutions, the enhancement in M_L is within a factor of three (for $w_U < 0.1$).

As the calibration curve for the SEC analysis used PS standards in M_w range from 0.390 to $3.69 \times 10^3 \text{ kg}\cdot\text{mol}^{-1}$, the measurements cannot resolve MWD for any PS chains of significantly higher molecular weight ($>3.69 \times 10^3 \text{ kg}\cdot\text{mol}^{-1}$). Although it is possible that the measurements shown in Figure

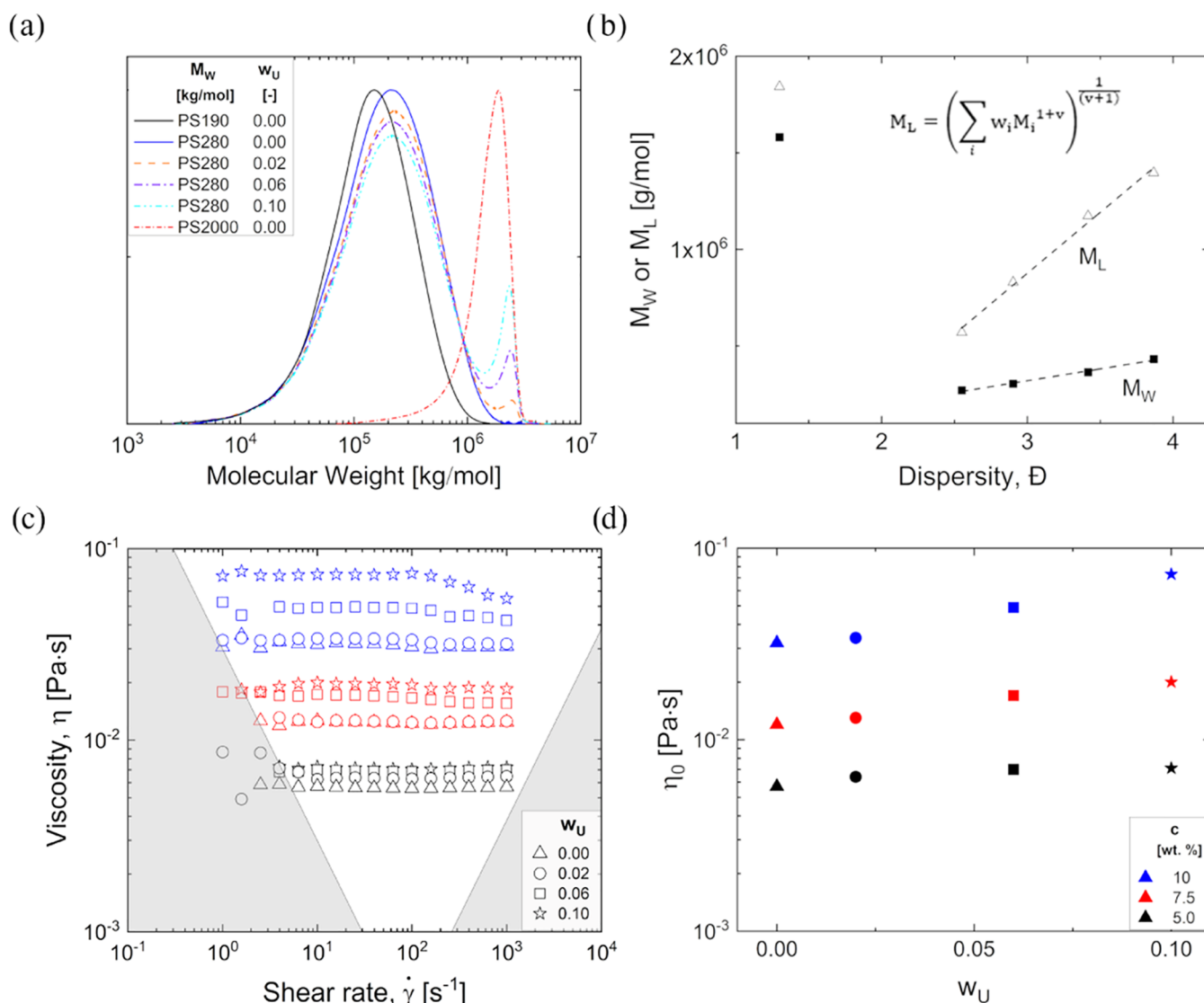


Figure 3. Influence of the UHM_w fraction on average molecular weight and shear viscosity. (a) Molecular weight distribution was determined using GPC for the three as-received PS samples (PS190, PS280, and PS2000) and bidisperse mixtures. (b) Weight-averaged molecular weight, M_w , and extensibility-averaged molecular weight, M_L , as a function of dispersity. (c) Steady shear viscosity as a function of shear rate for three polymer concentrations, with each group of four showing the weight fraction of the UHM_w component corresponding to symbols shown. (d) Zero-shear viscosity for a fixed total polymer concentration shows a mild increase as a function of w_U .

3a for PS2000 and bidisperse blends are representative of the underlying MWD and we know that some synthesis and separation strategies can generate such skewed distributions,^{83,84} the averages and distributions computed for solutions containing the UHM_w component might be approximate. The plausible uncertainty in values obtained from the SEC data does not alter the observations about the significant influence of the UHM_w component on viscosity, fiber diameter, fiber properties, and spinnability, as discussed next.

Figure 3c shows the measured, steady shear viscosity as a function of shear rate for UHM_w weight fraction, employed at three different polymer concentrations as the spinning dope. Figure 3d shows that increasing the UHM_w fraction leads to a proportional increase in zero-shear viscosity, η_0 , though increasing the total polymer concentration leads to a more substantial increase than obtained by changing the weight fraction of PS2000, w_U , over the limited range used in this study ($w_U < 0.1$). The influence of the UHM_w fraction on the

processing behavior cannot be elucidated completely by the measurements shown, as the shear rates encountered within the nozzle are typically higher (including for this study). Additionally, large extensional deformation fields arise both in converging channels as fluid is pushed into the nozzle and during the fiber spinning operations. The emergence of elastic instabilities and secondary flows for highly elastic fluids, including entangled polymer solutions (and melts), limits the range of shear rates employed in torsional rheometry measurements.⁸⁵ On the other hand, the highly nonlinear extensional rheology response is both challenging to characterize and cannot be estimated or predicted with the knowledge of the shear rheology response.^{69,85–87} Nevertheless, the datasets included in Figure 3c,d provide a first-order estimate of the influence of the UHM_w component on flow behavior and help to assess the degree of coil overlap and entanglements and their impact on spinnability, as discussed later.

Figure 4 highlights the influence of the UHM_w component on the fiber formation and morphology. Each row shows the

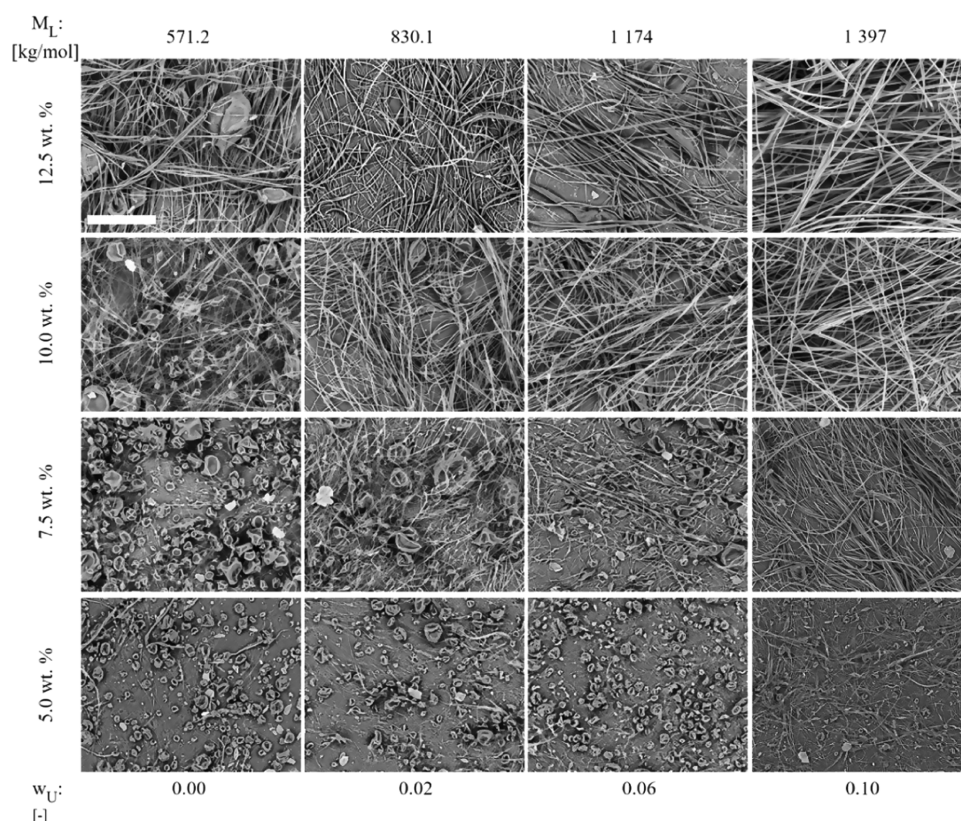


Figure 4. SEM images of the centrifugally spun PS fiber mats. Each row shows fibers spun from a spinning dope with matched polymer concentrations. However, the variation in the weight fraction of the UHM_w component leads to an increase in average molecular weight (left to right). In contrast, each column compares the influence of the total polymer concentration for fixed extensibility and dispersity. The scale bar is 100 μm.

SEM micrograph of centrifugally spun fibers formed for a fixed polymer concentration, with w_U and M_L values increasing from left to right. Similar enhancement of electrospinnability with added UHM_w fraction was demonstrated before^{4,39,40} but M_L as the critical parameter was first introduced in the study of electrospun PMMA fibers.⁴⁰ Independently, Fang et al.^{20,21} showed that adding <600 ppm of poly(ethylene oxide) (PEO, UHM_w with $M_w = 10^6$ g·mol⁻¹) to a thiol-ene monomer mix facilitates continuous fiber formation in reactive CFS that relies on UV polymerization for sol-gel-fiber transformation. Since the addition of dilute PEO solutions to monomer-mixed solvents had only marginal influence on shear viscosity, whereas CaBER measurements showed significant changes in pinching rate and time, as revealed by the analysis of the radius evolution data, the improved spinnability was attributed to an enhancement in extensional viscosity.^{20,21}

In addition to influencing spinnability and changing the fiber morphology, the UHM_w fraction improves sorption and mechanical properties. Figure 5a shows that the average fiber diameter for a fixed polymer concentration increases with the ultrahigh fraction. A stronger influence is observed for spinning dope prepared with a higher concentration. Next, we show that the influence of changing UHM_w weight fraction at fixed c or changing c at fixed M_w can be analyzed in terms of a combined dimensionless variable as follows. Increasing w_U leads to an increase in M_w and intrinsic viscosity, $[\eta]$, or a decrease in overlap concentration, $c^* \approx 1/[\eta]$, or using Graessley's arguments, $c^* = 0.77/[\eta]$. The change in intrinsic viscosity can be estimated using the Mark-Houwink-Sakurada equation, $[\eta] = KM^a$. Since the reported values of both K

and a vary over some range (say a lies in the range 0.69–0.73), we focus on pragmatic estimates made with the same values we utilized for SEC analysis (with $a = 0.7$). For a fixed polymer concentration, increasing the UHM_w component enhances M_w and increases the magnitude of scaled concentration, cKM^a , or Berry number. Thus, the matrix component, PS, with $M_w = 280$ kg·mol⁻¹, has estimated $c^* = 0.84$ wt % obtained with $c^* = 0.77/[\eta]$ (and a slightly higher value of $c^* = 1.1$ wt % is obtained for $c^* = 1/[\eta]$). Using $c^* = 0.77/[\eta]$, we obtain $c^* = 1.1$ wt % consistent with the value reported in our previous report on PS190, and hence we use this formula for estimating overlap concentration hereafter. On addition of UHM_w fraction with $w_U = 0.1$, the estimated overlap concentrations, $c^* = 0.6$ wt %, shift to a lower value.

Figure 5b shows that the measured diameter appears to increase with the Berry number, showing nearly quadratic dependence for the bidisperse, extensibility-enriched solutions, and a stronger power law for the fibers made from entangled PS190 solutions (shown as filled squares). The data points for beaded fibers are included as half-open symbols to show the distinction between beaded and continuous fibers. We find that the addition of the UHM_w fraction to PS280 leads to a substantial decrease in spinnable concentrations and fiber diameter in comparison with PS190. Decrease in concentration and viscosity of the spinning dope and smaller diameter of spun fibers are all desirable outcomes and show the significance of understanding the role of the UHM_w fraction and associated changes in extensibility and dispersity. Even though the correlation between the zero-shear viscosity and Berry number can be anticipated by considerations of linear

Table 2. Mechanical Properties of PS Fiber Mats Obtained by Tensile Tests carried out Using Fiber Mats Obtained under Similar Processing Conditions on the Bespoke CFS Setup, Designed to Obtain Highly Oriented Filaments

weight fraction of PS2000	tensile strength (MPa)	Young's modulus (MPa)	extension-at-break (%)	toughness ($\text{kJ}\cdot\text{m}^{-3}$)
0	0.66 ± 0.32	9.67 ± 5.37	11.35 ± 3.31	12.37 ± 5.91
0.02	0.94 ± 0.15	15.19 ± 4.59	8.08 ± 2.20	20.91 ± 4.62
0.06	1.19 ± 0.96	21.23 ± 5.84	9.60 ± 1.91	29.53 ± 6.68
0.10	1.35 ± 0.12	19.40 ± 3.11	13.02 ± 4.72	34.17 ± 5.07

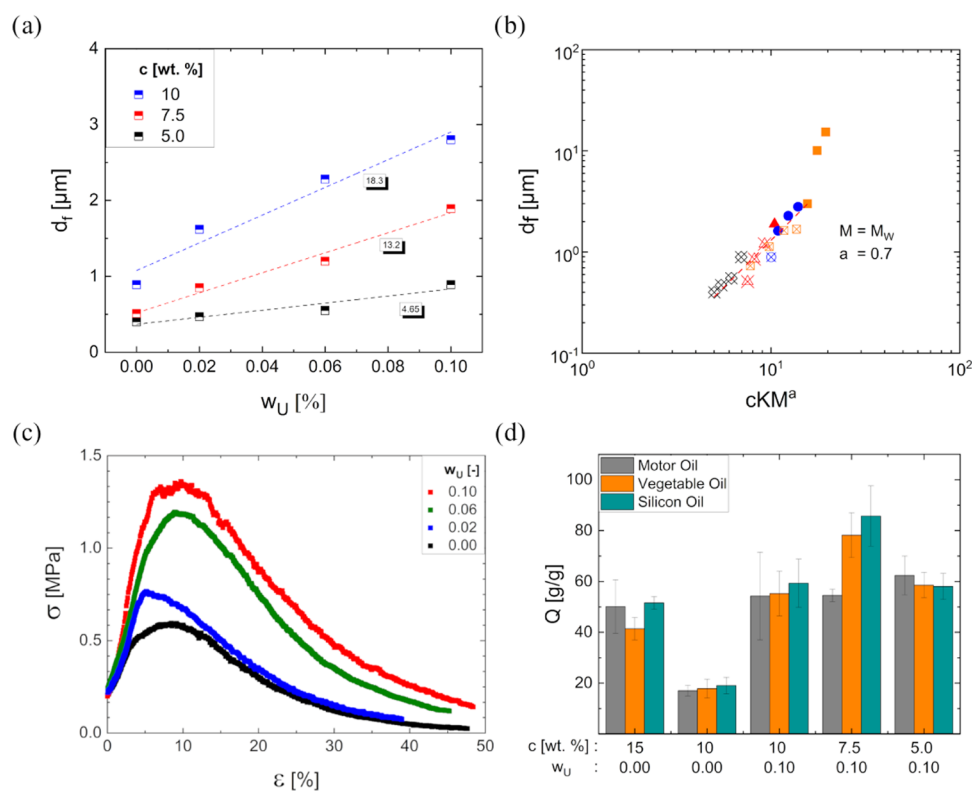


Figure 5. Morphology, mechanical properties, and sorption behavior. (a) Influence of the UHM_w fraction on fiber diameter becomes stronger at higher polymer concentrations. (b) Diameter vs rescaled concentration is shown for weight-averaged molecular weight, assuming exponent $a = 0.7$ for $M = M_w$. (c) Stress–strain curves obtained for $c = 10$ wt % reveal that the UHM_w fraction enhances modulus, strength, and toughness. (d) Sorption capacity, Q , expressed in [g/g] of five centrifugally spun fiber mats, is measured and contrasted for three motor oil, vegetable oil, and silicone oil.

viscoelasticity theory of the polymer solutions (as discussed in a later section), the diameter is also influenced both by the highly nonlinear rheological response of polymer solutions to complex deformation fields and concentration changes due to evaporative loss from the spiraling jet.

The addition of the UHM_w fraction leads to significant improvement in mechanical properties, characterized using tensile testing of the centrifugally spun fiber mats. Figure 5c shows the plot of measured tensile stress as a function of applied strain. Analysis of the stress–strain plots was carried out to determine Young's modulus, tensile strength, elongation-at-break, and toughness, and these values are listed in Table 2. The slope of the stress–strain curve in the low strain limit provides a measurement of the modulus, the peak value quantifies the tensile strength, and the area under the curve signifies toughness. Increasing the UHM_w fraction leads to a progressive enhancement in tensile strength (0.66–1.35 MPa), Young's modulus ($E = 9.67$ – 19.23 MPa), and toughness (12.37 – 34.17 $\text{kJ}\cdot\text{m}^{-3}$). Even at relatively low $w_U = 0.1$, all three measures are double the $w_U = 0$ polymer fiber values. Although the mechanical properties of PS fibers

without the UHM_w additive are comparable to the literature values for electrospun^{73,88} and centrifugally spun fiber mats,⁸¹ we find that the extensibility enrichment leads to a significant increase in the tensile strength of fiber mats. The bespoke CFS setup used here allows us to obtain aligned filaments, and by matching both the processing conditions and the mechanical testing protocols, we sought to make these comparisons more robust.

Figure 5d shows the oil sorption capacity, Q , measured for the fiber mats, as a function of the indicated PS concentration for $w_U = 0$ or 0.1 to highlight the influence of the UHM_w component. The continuous fiber mats ($c = 15$ wt %) formed using PS280 solutions (with $w_U = 0$) show a significantly higher oil uptake than the beaded fiber mats ($c = 10$ wt %). For the fiber mats formed using bidisperse mixtures with matched polymer concentration ($c = 10$ wt %), the $w_U = 0.1$ nonwovens show much higher Q values. Figure 4 shows that adding the UHM_w component or extensibility enrichment leads to a change in the fiber morphology from beaded to continuous fibers. Even though the filaments appear thinner in the presence of beads, the overall oil uptake is lower. The Q values

shown in Figure 5d compare well with the sorption capacity of electrospun PS fiber mats, including those spun with THF as a solvent and those characterized for determining pore sizes.^{77–82,89} Fascinatingly, the values are significantly higher than the values reported for oil sorption capacity by commercial nonwovens made with polypropylene (PP) (usual range $\sim 15\text{--}30\text{ g}\cdot\text{g}^{-1}$) and by natural materials like cotton that show higher sorption capacity ($Q \sim 20\text{--}40\text{ g}\cdot\text{g}^{-1}$) than wool and sisal ($8\text{--}15\text{ g}\cdot\text{g}^{-1}$).^{77–82,89–91} Although the sorption tests emulate the protocols used in previous studies,^{77–82,89,91} designing cost-effective and pragmatic sorbents with PS nonwovens would benefit from a careful assessment of the influence of porosity, superhydrophobicity, and the orientation–structure properties of fibers. Previous studies show that the size and number density of pores depend on humidity and airflow conditions,^{74,92} but the mechanism for the formation of pores is not completely understood, and the influence of the UHM_w additive on porosity requires future investigation. Pore formation is often attributed to mechanisms based on phase separation,^{74,89,92,93} even though qualitative features are also reminiscent of the breath-figure-templated assembly (BFTA) of pores in “holey” polymer films in volatile polymer solutions exposed to moist air.^{94–97} We leave the pursuit of a more detailed investigation of porosity, mechanism of pore formation, and the influence of pores on fiber properties for future studies. Here, we focus on describing how spinnability depends on average extensibility that can be tuned by adding the ultrahigh molecular weight polymer component.

DISCUSSION

Figure 6a plots zero-shear viscosity of solutions of as-received and extensibility-enriched polymers against the Berry number, $c[\eta] = cKM_w^a$. The collapse of zero-shear viscosity data follows the universalities and scaling theories as anticipated for semidilute solutions of flexible polymers like polystyrene.^{63,67,98–102} The plots include data for a subset of extensibility-enriched solutions (PS280 with UHM_w PS2000) (see Figure 3c,d for viscosity vs shear rate and w_U , respectively) and also incorporate the data for PS190 that were centrifugally spun under matched spinning conditions.⁴⁸ In addition to requiring a higher degree of chain overlap, PS190 solutions have a much higher zero-shear viscosity. The highly entangled spinnable PS190 solutions that correspondingly have higher Berry numbers (>10) exhibit significant shear thinning at high shear rates relevant for flows within the nozzle. In contrast, in Figure 3c, except for 10 wt % solutions with $w_U = 0.06$ (blue stars) and $w_U = 0.1$ (blue squares), most solutions show rate-independent viscosity, reminiscent of constant viscosity, elastic fluids known as Boger fluids.^{103–105} Typically, Boger fluids are dilute polymer solutions formulated in oligomeric or high-viscosity solvents.^{103–105} However, the viscosity values and the estimates for overlap and entanglement concentrations as well as additional datasets included only in Figure 6b indicate that several of the extensibility-enriched solutions are in the unentangled, semidilute regime, in addition to solutions in the entangled regime.

The macromolecular contribution to shear viscosity for unentangled solutions can be estimated using $\eta_p \approx G\lambda$, with $G \approx \phi k_B T / N_K b_K^3$ for both dilute and semidilute solutions.¹⁰⁰ In contrast with the linear law, $\eta_p \propto \phi^1$, obtained for the dilute solutions of flexible polymers, the semidilute solutions display $\eta_{sp} = (c/c^*)^{1/(3\nu-1)}$ for unentangled and much stronger concentration dependence with $\eta_{sp} = (c/c^*)^{3/(3\nu-1)}$ above the

entanglement concentration, c_e , due to the role played by topological interactions (or entanglements). For the flexible polymer in a good solvent, an exponent of 3.9 is anticipated¹⁰⁰ that compares quite well with the observed value of 3.8. For the extensibility-enriched samples, the concentration-dependent variation in shear viscosity corresponding to the entangled regime seems to extend right down to the estimated value of Berry number of 6.9 (estimated using an entanglement concentration value, computed using the weight-averaged polymer molecular weight). Viscosity vs concentration plot reveals that many spinnable, extensibility-enriched solutions are in the entangled regime, as anticipated from previous studies that argue that entanglements facilitate fiber formation.^{31–33,40,46}

However, Figure 6b summarizes the observations for the fiber morphology as a function of polymer concentration and the weight-averaged molecular weight, M_w , for a much broader range of concentrations than those characterized rheologically in Figures 3c,d and 6a. The transition from the beaded fiber into continuous fibers is shown by open and filled circles, respectively. The experimentally determined locus of points in $c\text{--}M_w$ plots corresponding to concentrations for the beaded-continuous fiber transition or c_{BC} for the centrifugally spun extensibility-enriched solutions (PS280 with UHM_w PS2000 added) displays a power law relation of $c_{BC} \sim M_w^{-1.44}$ that, on extrapolation, fails to capture the corresponding transition for as-received PS190 and PS2000. Both overlap and entanglement concentration display a much weaker concentration dependence, $c^* \sim M_w^{-a}$ and $c_e \sim M_w^{-a}$, than that displayed here. Although a relatively large number of studies associate entanglements with spinnability,^{31,33,38,41,46,48–50} our results echo findings included in a couple of electrospinning studies,^{39,41} showing that the c_{spin} can lie below c_e and disagree with the $c_{spin} \propto c_e \sim M_w^{-a}$ power law.

Even though the lower molecular weight, matrix component, PS with $M_w = 280\text{ kg}\cdot\text{mol}^{-1}$ has a high molecular weight in comparison with the PS entanglement molecular weight ($M_e = 17\text{ kg}\cdot\text{mol}^{-1}$ with $N_e = 23$ and Kuhn segment size, $b_K = 1.8\text{ nm}$), the Mark–Houwink–Sakurada expression for intrinsic viscosity gives an estimate of $c^* = 0.84\text{ wt } \%$, whereas the estimate for entanglement concentration using the expression $c_e/c^* = N_e^{3\nu-1}$ yields $c_e = 7.6\text{ wt } \%$ (see blue line in Figure 5b). On addition of UHM_w fraction with $w_U = 0.1$, the estimated overlap and entanglement concentrations, $c^* = 0.6\text{ wt } \%$ and $c_e = 5.6\text{ wt } \%$, shift to a lower value. Figure 6b shows that many CFS experiments carried out with concentrations below the computed entanglement concentration form fibers successfully. The observations and estimates suggest that extensibility enrichment facilitates spinnability even in the absence of entanglements.

Lastly, we revisit the processability diagram often drawn by plotting observed fiber morphologies (beads, BOAS, and continuous) on a $c\text{--}M_w$ coordinate space and reconstruct it using the extensibility-averaged molecular weight, M_L , as shown in Figure 7. In close agreement with the findings by Palangetic et al.,⁴⁰ we find that the minimal spinnable concentration for these high-extensibility and extensibility-enriched solutions displays $c_{spin} \sim M^{-(\nu+1)} \sim M^{-1.566}$. Quite significantly, we find that the boundary between beaded to continuous fibers can be fit by an expression of the form $c_{BC} \sim M_L^{-0.7}$. The scaling law appears to be consistent with $c_{BC} \sim M^{-(3\nu-1)}$, the PS-THF solutions, as $\nu = 0.57$ or $a = 3\nu - 1 = 0.7$ yields $c_{BC} \sim M_L^{-0.7}$. A close examination of Figure 6b shows

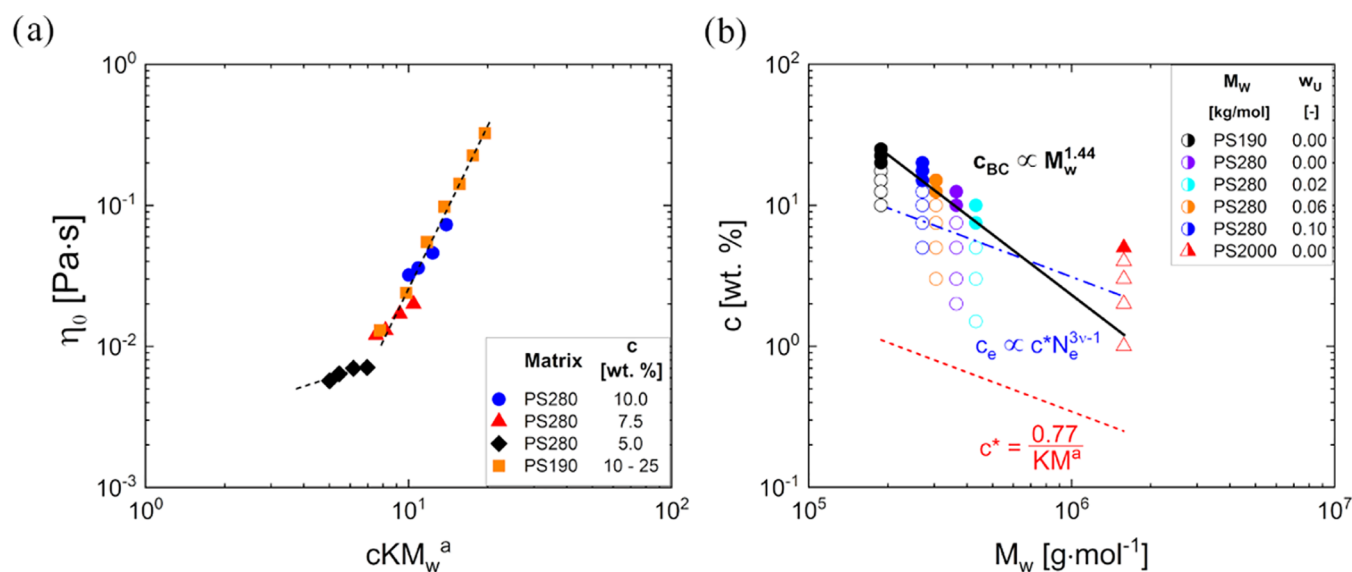


Figure 6. Spinning dope viscosity and the fiber diameter as functions of Berry number. (a) Zero-shear viscosity as a function of Berry number exhibits a power law dependence of 3.8 for PS190 solutions and for most of the extensibility-enriched PS280 solutions shown. (b) On the c – M_w plot, the beaded and continuous fibers are shown in open and closed symbols, respectively. The locus of concentrations capturing the beaded-continuous fiber transition or c_{BC} was fit for extensibility-enriched solutions to obtain the scaling relation with exponent 1.44. The black-line fit is extrapolated to show that as-received samples do not show the transition at the concentration anticipated by this law. The dotted red line shows the overlap concentration, c^* , whereas the blue dashed–dotted line corresponds to the estimated entanglement concentration, c_e . Increasing the fraction of the UHM $_w$ additive leads to extensibility enrichment and facilitates spinnability for $c < c_e$. A much more extensive range of polymer concentrations was explored in the spinning experiments. Hence, only a subset of points included in the c – M_w plot is shown in the viscosity vs concentration plot.

that the c_{spin} values lie in the unentangled regime, whereas the transition from beaded to continuous fibers occurs for entangled solutions.

The timescale for the growth of the surface tension-driven instabilities that lead to the formation of beaded fibers or beads is influenced by an interplay of capillarity and viscoelasticity,^{4,106–112} and the onset and initial growth of sinusoidal instability for a liquid cylinder are primarily influenced by the linear viscoelastic response.^{56,57,106,107,109,112–116} However, in the later stage, streamwise velocity gradients associated with extensional flows arise in capillarity-squeezed necks, and response to strong extensional flows, influenced by stretched chain hydrodynamics, including coil-stretch transition as well as finite extensibility effects, influence the dynamics.^{56,57,107,109–112,115,117,118} We recognize that the deformation history, including strong shear and extensional flows within the nozzle and during stretching of the jet, conformational changes of polymers, and evaporation also influence the growth and evolution of the instability and final pinching dynamics.^{50,115,117,119–122} Therefore, to the first order, we can ascribe c_{BC} (solid black line) in Figure 7 to the influence of higher viscosity and elasticity of entangled solutions on the onset and initial growth of instability, which is hence responsible for $c_{BC} \propto M_L^{-0.7}$.

In contrast, extensibility-enriched spinnability and the scaling observed for c_{spin} are dictated by the extensional rheology response, including high Trouton ratio and strain hardening of highly flexible polymers like PEO, PS, PAN, and PVP. We envision that in low extensibility but highly entangled solutions, both spinnability and continuous fiber formation rely on higher viscosity and higher elasticity of the entangled solutions and additionally, on a steep viscosity increase on the solvent loss that compensates for pronounced shear thinning and extensional thinning at intermediate rates.^{69,123–129}

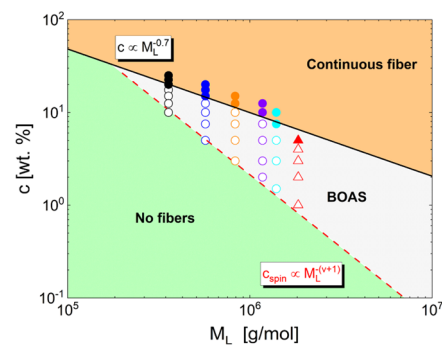


Figure 7. Extensibility-facilitated spinnability diagram. Three regimes can be distinguished in the plot of polymer concentration against extensibility-averaged molecular weight. Low c and low M_L lead to the formation of beads (green), intermediate concentrations correspond to the formation of the beaded fiber (BOAS) regime (gray), whereas the beaded-continuous transition, c_{BC} , is demarcated by a bold black line, with the continuous fiber regime (orange) displayed at a higher concentration.

Although Palangetic et al.⁴⁰ showed $c_{spin} \sim M^{-(\nu+1)} \sim M^{-1.566}$ describes the minimum concentration required for electrospinning, a closer examination of the datasets they considered shows that two regimes could be identified corresponding to $c_{spin} \sim M^{-(3\nu-1)}$ and $c_{spin} \sim M^{-(\nu+1)}$ for low and high molecular weight systems. Malkin et al.⁴¹ argued that spinnability on a c – M plot (see Figure 18 in their article) has three regimes: (a) $c \propto M^{-0.7}$ for solutions with lower molecular weight, identified with the entanglement concentration, (b) $c \propto M^{-1}$ an intermediate regime for the semidilute polymer attributed to the role of phase separation under extension, and (c) $c \propto M^{-2}$ due to the extensional viscosity of extended chains, by assuming the influence of the coil-stretch transition. Malkin

et al.⁴¹ suggested that it was difficult to distinguish between their scaling and that presented by Palangetic et al.⁴⁰ due to the lack of sufficient data for extended range but presented PEO solution spinnability data to argue that c_{spin} could scale with M^{-2} .

We contend that minimum spinnable concentration could be described in at least two prototypical ways, irrespective of the spinning method (electrospinning, dry jet, or centrifugal spinning). Type 1 polymer solutions display extensional viscosity with significant strain hardening and high Trouton ratios and significantly delay pinching compared to a Newtonian fluid of the same viscosity.^{39–41,55–68,101,107–111,118,130} The high flexibility polymers like PEO, PVA, and PVP with high molecular weight can satisfy the high extensibility or extensibility-enriched (EE) and large Trouton ratio criteria, and these form fibers above c_{spin} as anticipated by Palangetic et al.⁴⁰ and later discussed by Malkin et al.⁴¹ Type 2 polymer solutions, due to lower M_w or lower extensibility, rely on the role of entanglements and volatility for a delayed onset and slower growth of capillarity-driven instability as well as on the rapid viscosity enhancement during the drying process. Both together make the volatile entangled (VE) polymer solutions more suitable for fiber spinning as the zero shear viscosity values are high enough to delay the onset of instability, and the subsequent loss of solvent leads to a pronounced viscosity enhancement with biquadratic or stronger power laws. Arguably, this explains the origin of the $c_{\text{spin}} \propto c_e \propto M^{-0.7}$ scaling used and discussed often in many ES and CFS studies that relied on spinning fibers with entangled solutions of intermediate molecular weight (and low extensibility) polymers.^{31–33,38,42,46,48–50,131,132}

A relatively recent study¹³³ of steady extensional viscosity values measured for entangled solutions of relatively monodisperse PS in theta solutions found that $\eta_E \propto M_w \sqrt{c}$, implying that the extensional viscosity shows a weaker dependence on concentration in entangled solutions than that observed in dilute solutions. By accounting for the solvent quality, the corresponding concentration dependence leads to an expression of the form $\eta_E \propto c^\nu M_w$, in contrast to the scaling behavior for c_{BC} in extensibility-enriched systems and c_{spin} in low extensibility, highly entangled systems.^{40,64,66} However, stronger flows that can arise in pinching necks in the late stage are primarily governed by the extensional rheology response and determine the minimal spinnable concentration if a significant difference exists in shear and extensional rheology response (especially for highly flexible, large-extensibility polymers). We mention this with the caveat that due to the complex deformation history within the nozzle and during travel from the nozzle to a collector, direct comparisons with any extensional rheology measurements remain as challenging now as ever before.^{28,29,55,63–71,87,101,133–135} Nevertheless, we find that the locus of transition concentrations or c_{spin} and c_{BC} are both influenced by the extensional rheology response and display the observed and tunable sensitivity to extensibility and dispersity.

Improving electrospinnability by adding ultrahigh molecular weight polymers facilitated spinning protein fibers for food applications^{47,136} and spinning fibers from polysaccharides like chitosan and sodium alginate.^{34,43,131,137,138} The observed improvements can be classified as examples of extensibility-enriched spinnability. The addition of the UHM_w PEO fraction to polysaccharide solutions changes the extension rheology response due to higher extensibility, L_E , of poly(ethylene

oxide) compared to polysaccharides. Dinic and Sharma showed that higher L_E leads to much longer extensional relaxation time and higher extensional viscosity for unentangled PEO solutions even if shear viscosity and coil size match HEC.^{64–66} Our extensive characterization of the extensional rheology response of unentangled solutions of flexible and semiflexible polymers has revealed that the degree of strain hardening, coil-stretch physics, response to capillarity-driven pinching flows, and extensibility-dependent filament lifespan are sensitive to polymer chemistry and flexibility, extensibility, and segmental dissymmetry (ratio of Kuhn length to packing length, as detailed elsewhere).^{63–68,71,130} We anticipate this recent progress in deciphering and understanding the influence of the chemical structure on extensional rheology of dilute and semidilute polymers and contrasting with the case of entangled polymer solutions^{69,85,86,123–128} will continue to shed more light on spinnability for Type 1 and Type 2 systems, assuming that the processing conditions that determine the deformation rates and deformation history are accounted for and controlled.

CONCLUSIONS

We find that the addition of relatively low volume fraction ultrahigh molecular weight (UHM_w) polystyrene (PS) with $M_w = 2000 \text{ kg}\cdot\text{mol}^{-1}$ (quoted by the supplier) to spinning dope formulated with the matrix PS with $M_w = 280 \text{ kg}\cdot\text{mol}^{-1}$ leads to the formation of beaded fibers and the transition from beaded to continuous fibers at lower polymer concentrations. For example, the weight fraction, $w_U < 0.1$, of UHM_w fraction shifts the minimum spinnable concentration from $c = 15 \text{ wt } \%$ to as low as $c = 7.5 \text{ wt } \%$. We find that the resulting fiber mats showed both enhanced mechanical properties and sorption capacity for three different oils. The marginal enhancement in zero-shear viscosity on varying UHM_w fraction or total polymer concentration (for any UHM_w fraction) follows a universal power law increase with the overlap parameter or the Berry number if intrinsic viscosity or overlap concentrations are computed using the weight-averaged molecular weight determined from the SEC data. The scaling exponents are consistent with the behavior expected for entangled solutions, though bidisperse solutions appear to show the same exponent for all semidilute solutions above the Berry number of unity (for $c > c^*$). Significant changes in spinnability and fiber properties cannot be explained by examining only the shear rheology response. The processing conditions and solvent are kept constant for the range of polymer solutions examined here. The spiraling jet of fluid ejected from the nozzle undergoes stretching, bending, and capillarity-driven squeeze flow, creating streamwise velocity gradients associated with the extensional rheology response. Although shear viscosity is hardly influenced by the addition of small amounts of UHM_w fractions, the extensional rheology response is extremely sensitive to the size of stretched chains, and extensional viscosity depends on extensibility. Here, we show that the minimum spinnable concentration can be evaluated in terms of the extensibility-averaged molecular weight, M_L , using the same relationship, $c_{\text{spin}} \sim M_L^{-(\nu+1)} \sim M_L^{-1.566}$ reported earlier as an electrospinnability criterion for flexible polymers with high molecular weight.

Our experiments show that the transition of beaded fibers to continuous fibers displays a weaker dependence on the extensibility-averaged molecular weight, consistent with the exponent anticipated for entangled polymers but with M_w

replaced by M_L . We show that a spinnability diagram can be constructed using the polymer concentration and extensibility-averaged molecular weight for the PS/THF system and outline relationships that identify borders between beaded and beaded fibers (using c_{spin}) and between beaded and continuous fibers (c_{BC}). The influence of high molecular weight PEO on spinnability of polysaccharides, protein solutions, and even lower molecular weight PEO solutions or a reactive monomer solution in both electrospinning and centrifugal force spinning is rationalized here, and we find that extensibility-enriched solutions show enhanced spinnability, and the addition of the UHM_w component also influences mechanical and physico-chemical properties. We perceive this contribution as complementary to the published experimental and theoretical studies (including our own) aimed at elucidating the influence of the solvent choice and process parameters like spinning speed, nozzle shape and size, distance to the collector, and air flow on spinnability, fiber diameter, and morphology. We envision that our contribution will motivate us and others to investigate the influence of extensibility using polymeric systems with sterner control over the molecular weight distributions and complementary studies on the extensional rheology response of bidisperse systems. We anticipate that the spinnability diagram will provide a pragmatic solution to the problem of making nonwovens from a variety of polymers and the use of spinning dopes based on cheaper, lower molecular weight unused or recycled polymers, through understanding of extensibility-enriched (EE) spinnability.

AUTHOR INFORMATION

Corresponding Authors

Naveen K. Reddy – Institute for Materials research (IMO-IMOMEC), Hasselt University, B-3590 Diepenbeek, Belgium; IMEC vzw-Division IMOMEC, B-3590 Diepenbeek, Belgium; orcid.org/0000-0003-0163-485X; Email: naveen.reddy@uhasselt.be

Vivek Sharma – Department of Chemical Engineering, University of Illinois Chicago, Chicago, Illinois 60607, United States; orcid.org/0000-0003-1152-1285; Email: viveks@uic.edu

Author

Jorgo Merchiers – Institute for Materials research (IMO-IMOMEC), Hasselt University, B-3590 Diepenbeek, Belgium; IMEC vzw-Division IMOMEC, B-3590 Diepenbeek, Belgium

Complete contact information is available at:

<https://pubs.acs.org/10.1021/acs.macromol.1c02164>

Notes

The authors declare no competing financial interest.

ACKNOWLEDGMENTS

The authors (J.M. and N.K.R.) acknowledge the IMO-IMOMEC at the University of Hasselt for providing financial support. V.S. acknowledges funds from the 3M nontenured faculty award (NFTA). The authors also acknowledge discussions with students from the ODES lab at the UIC, especially Carina Martinez and Cheryl Slykas. The authors thank Dr. Samanvaya Srivasatava (UCLA) and Dr. Amanda Marciel (Rice) for their comments on the draft.

REFERENCES

- (1) Gupta, V. B.; Kothari, V. K. *Manufactured Fiber Technology*; Chapman & Hall: London, 1997.
- (2) Ziabicki, A. *Fundamentals of Fibre Formation*; John Wiley & Sons: New York, 1976.
- (3) Li, D.; Xia, Y. Electrospinning of nanofibers: reinventing the wheel? *Adv. Mater.* **2004**, *16*, 1151–1170.
- (4) Park, J. H.; Rutledge, G. C. 50th anniversary perspective: advanced polymer fibers: high performance and ultrafine. *Macromolecules* **2017**, *50*, 5627–5642.
- (5) Atıcı, B.; Ünlü, C. H.; Yanilmaz, M. A review on centrifugally spun fibers and their applications. *Polym. Rev.* **2021**, 1–64.
- (6) Rogalski, J. J.; Bastiaansen, C. W.; Peijs, T. Rotary jet spinning review—a potential high yield future for polymer nanofibers. *Nanocomposites* **2017**, *3*, 97–121.
- (7) Barhoum, A.; Pal, K.; Rahier, H.; Uludag, H.; Kim, I. S.; Bechelany, M. Nanofibers as new-generation materials: from spinning and nano-spinning fabrication techniques to emerging applications. *Appl. Mater. Today* **2019**, *17*, 1–35.
- (8) Dos Santos, D. M.; Correa, D. S.; Medeiros, E. S.; Oliveira, J. E.; Mattoso, L. H. C. Advances in functional polymer nanofibers: From spinning fabrication techniques to recent biomedical applications. *ACS Appl. Mater. Interfaces* **2020**, *12*, 45673–45701.
- (9) Yoon, K.; Hsiao, B. S.; Chu, B. Functional nanofibers for environmental applications. *J. Mater. Chem.* **2008**, *18*, 5326–5334.
- (10) Venugopal, J.; Ramakrishna, S. Applications of polymer nanofibers in biomedicine and biotechnology. *Appl. Biochem. Biotechnol.* **2005**, *125*, 147–157.
- (11) Doshi, J.; Reneker, D. H. Electrospinning process and applications of electrospun fibers. *J. Electrostatics* **1995**, *35*, 151–160.
- (12) Ellison, C. J.; Phatak, A.; Giles, D. W.; Macosko, C. W.; Bates, F. S. Melt blown nanofibers: Fiber diameter distributions and onset of fiber breakup. *Polymer* **2007**, *48*, 3306–3316.
- (13) Banerji, A.; Jin, K.; Mahanthappa, M. K.; Bates, F. S.; Ellison, C. J. Porous fibers templated by melt blowing cocontinuous immiscible polymer blends. *ACS Macro Lett.* **2021**, *10*, 1196–1203.
- (14) Stojanovska, E.; Canbay, E.; Pampal, E. S.; Calisir, M. D.; Agha, O.; Polat, Y.; Simsek, R.; Gundogdu, N. S.; Akgul, Y.; Kilic, A. A review on non-electro nanofibre spinning techniques. *RSC Adv.* **2016**, *6*, 83783–83801.
- (15) Sarkar, K.; Gomez, C.; Zambrano, S.; Ramirez, M.; de Hoyos, E.; Vasquez, H.; Lozano, K. Electrospinning to forcesspinning. *Mater. Today* **2010**, *13*, 12–14.
- (16) Badrossamay, M. R.; McIlwee, H. A.; Goss, J. A.; Parker, K. K. Nanofiber assembly by rotary jet-spinning. *Nano Lett.* **2010**, *10*, 2257–2261.
- (17) Pham, Q. P.; Sharma, U.; Mikos, A. G. Electrospinning of polymeric nanofibers for tissue engineering applications: a review. *Tissue Eng.* **2006**, *12*, 1197–1211.
- (18) Chavez, R. O.; Lodge, T. P.; Alcoutlabi, M. Recent developments in centrifugally spun composite fibers and their performance as anode materials for lithium-ion and sodium-ion batteries. *Mater. Sci. Eng., B* **2021**, *266*, No. 115024.
- (19) Xu, H.; Chen, H.; Li, X.; Liu, C.; Yang, B. A comparative study of jet formation in nozzle-and nozzle-less centrifugal spinning systems. *J. Polym. Sci., Part B: Polym. Phys.* **2014**, *52*, 1547–1559.
- (20) Fang, Y.; Dulaney, A. D.; Gadley, J.; Maia, J. M.; Ellison, C. J. Manipulating characteristic timescales and fiber morphology in simultaneous centrifugal spinning and photopolymerization. *Polymer* **2015**, *73*, 42–51.
- (21) Fang, Y.; Dulaney, A. R.; Gadley, J.; Maia, J.; Ellison, C. J. A comparative parameter study: Controlling fiber diameter and diameter distribution in centrifugal spinning of photocurable monomers. *Polymer* **2016**, *88*, 102–111.
- (22) Weitz, R. T.; Harnau, L.; Rauschenbach, S.; Burghard, M.; Kern, K. Polymer nanofibers via nozzle-free centrifugal spinning. *Nano Lett.* **2008**, *8*, 1187–1191.

- (23) Noroozi, S.; Alamdari, H.; Arne, W.; Larson, R. G.; Taghavi, S. M. Regularized string model for nanofiber formation in centrifugal spinning methods. *J. Fluid Mech.* **2017**, *822*, 202–234.
- (24) Noroozi, S.; Arne, W.; Larson, R. G.; Taghavi, S. M. A comprehensive mathematical model for nanofiber formation in centrifugal spinning methods. *J. Fluid Mech.* **2020**, *892*, No. A26.
- (25) Ren, L.; Ozisik, R.; Kotha, S. P.; Underhill, P. T. Highly efficient fabrication of polymer nanofiber assembly by centrifugal jet spinning: process and characterization. *Macromolecules* **2015**, *48*, 2593–2602.
- (26) Padron, S.; Fuentes, A.; Caruntu, D.; Lozano, K. Experimental study of nanofiber production through forcesspinning. *J. Appl. Phys.* **2013**, *113*, No. 024318.
- (27) Zhang, X.; Lu, Y. Centrifugal spinning: an alternative approach to fabricate nanofibers at high speed and low cost. *Polym. Rev.* **2014**, *54*, 677–701.
- (28) Petrie, C. J. S. One hundred years of extensional flow. *J. Non-Newtonian Fluid Mech* **2006**, *137*, 1–14.
- (29) Petrie, C. J. S.; Petrie, A. Spinning viscosity. *J. Non-Newtonian Fluid Mech.* **1995**, *57*, 83–101.
- (30) Larson, R. G. Spinnability and viscoelasticity. *J. Non-Newtonian Fluid Mech.* **1983**, *12*, 303–315.
- (31) Gupta, P.; Elkins, C.; Long, T. E.; Wilkes, G. L. Electrospinning of linear homopolymers of poly (methyl methacrylate): exploring relationships between fiber formation, viscosity, molecular weight and concentration in a good solvent. *Polymer* **2005**, *46*, 4799–4810.
- (32) Shenoy, S. L.; Bates, W. D.; Frisch, H. L.; Wnek, G. E. Role of chain entanglements on fiber formation during electrospinning of polymer solutions: good solvent, non-specific polymer–polymer interaction limit. *Polymer* **2005**, *46*, 3372–3384.
- (33) McKee, M. G.; Wilkes, G. L.; Colby, R. H.; Long, T. E. Correlations of solution rheology with electrospun fiber formation of linear and branched polyesters. *Macromolecules* **2004**, *37*, 1760–1767.
- (34) Rošic, R.; Pelipenko, J.; Kocbek, P.; Baumgartner, S.; Bešter-Rogač, M.; Kristl, J. The role of rheology of polymer solutions in predicting nanofiber formation by electrospinning. *Eur. Polym. J.* **2012**, *48*, 1374–1384.
- (35) Jarusuwannapoom, T.; Hongrojjanawiwat, W.; Jitjaicham, S.; Wannatong, L.; Nithitanakul, M.; Pattamaprom, C.; Koombhongse, P.; Rangkupan, R.; Supaphol, P. Effect of solvents on electrospinnability of polystyrene solutions and morphological appearance of resulting electrospun polystyrene fibers. *Eur. Polym. J.* **2005**, *41*, 409–421.
- (36) Nitanan, T.; Opanasopit, P.; Akkaramongkolporn, P.; Rojanarata, T.; Ngawhirunpat, T.; Supaphol, P. Effects of processing parameters on morphology of electrospun polystyrene nanofibers. *Korean J. Chem. Eng.* **2012**, *29*, 173–181.
- (37) Uyar, T.; Besenbacher, F. Electrospinning of uniform polystyrene fibers: The effect of solvent conductivity. *Polymer* **2008**, *49*, 5336–5343.
- (38) Wang, C.; Hsu, C.-H.; Lin, J.-H. Scaling laws in electrospinning of polystyrene solutions. *Macromolecules* **2006**, *39*, 7662–7672.
- (39) Yu, J. H.; Fridrikh, S. V.; Rutledge, G. C. The role of elasticity in the formation of electrospun fibers. *Polymer* **2006**, *47*, 4789–4797.
- (40) Palangetic, L.; Reddy, N. K.; Srinivasan, S.; Cohen, R. E.; McKinley, G. H.; Clasen, C. Dispersity and spinnability: Why highly polydisperse polymer solutions are desirable for electrospinning. *Polymer* **2014**, *55*, 4920–4931.
- (41) Malkin, A. Y.; Semakov, A. V.; Skvortsov, I. Y.; Zatonikhin, P.; Kulichikhin, V. G.; Subbotin, A. V.; Semenov, A. N. Spinnability of dilute polymer solutions. *Macromolecules* **2017**, *50*, 8231–8244.
- (42) Subramanian, C.; Weiss, R. A.; Shaw, M. T. Electrospinning and characterization of highly sulfonated polystyrene fibers. *Polymer* **2010**, *51*, 1983–1989.
- (43) Mengistu Lemma, S.; Bossard, F.; Rinaudo, M. Preparation of pure and stable chitosan nanofibers by electrospinning in the presence of poly (ethylene oxide). *Int. J. Mol. Sci.* **2016**, *17*, No. 1790.
- (44) Lundahl, M. J.; Berta, M.; Ago, M.; Stading, M.; Rojas, O. J. Shear and extensional rheology of aqueous suspensions of cellulose nanofibrils for biopolymer-assisted filament spinning. *Eur. Polym. J.* **2018**, *109*, 367–378.
- (45) Koepfel, A.; Laity, P. R.; Holland, C. Extensional flow behaviour and spinnability of native silk. *Soft Matter* **2018**, *14*, 8838–8845.
- (46) Haward, S. J.; Sharma, V.; Butts, C. P.; McKinley, G. H.; Rahatekar, S. S. Shear and extensional rheology of cellulose/ionic liquid solutions. *Biomacromolecules* **2012**, *13*, 1688–1699.
- (47) Kutzli, I.; Gibis, M.; Baier, S. K.; Weiss, J. Electrospinning of whey and soy protein mixed with maltodextrin—Influence of protein type and ratio on the production and morphology of fibers. *Food Hydrocolloids* **2019**, *93*, 206–214.
- (48) Merchiers, J.; Meurs, W.; Deferme, W.; Peeters, R.; Buntinx, M.; Reddy, N. K. Influence of polymer concentration and nozzle material on centrifugal fiber spinning. *Polymers* **2020**, *12*, No. 575.
- (49) Merchiers, J.; Martínez Narváez, C. D. V.; Slykas, C.; Buntinx, M.; Deferme, W.; D’Haen, J.; Peeters, R.; Sharma, V.; Reddy, N. K. Centrifugally spun PEO fibers rival the properties of electrospun fibers. *J. Polym. Sci.* **2021**, *59*, 2754–2762.
- (50) Merchiers, J.; Martínez Narváez, C. D. V.; Slykas, C.; Reddy, N. K.; Sharma, V. Evaporation and rheology chart the processability map for centrifugal force spinning. *Macromolecules* **2021**, 11061–11073.
- (51) Tripathi, A.; Whittingstall, P.; McKinley, G. H. Using filament stretching rheometry to predict strand formation and “processability” in adhesives and other non-Newtonian fluids. *Rheol. Acta* **2000**, *39*, 321–337.
- (52) Taghavi, S. M.; Larson, R. G. Regularized thin-fiber model for nanofiber formation by centrifugal spinning. *Phys. Rev. E* **2014**, *89*, No. 023011.
- (53) Golecki, H. M.; Yuan, H.; Glavin, C.; Potter, B.; Badrossamay, M. R.; Goss, J. A.; Phillips, M. D.; Parker, K. K. Effect of solvent evaporation on fiber morphology in rotary jet spinning. *Langmuir* **2014**, *30*, 13369–13374.
- (54) Divvela, M. J.; Ruo, A.-C.; Zhmayev, Y.; Joo, Y. L. Discretized modeling for centrifugal spinning of viscoelastic liquids. *J. Non-Newtonian Fluid Mech.* **2017**, *247*, 62–77.
- (55) Nguyen, T. Q.; Kausch, H. H. *Flexible Polymer Chains in Elongational Flow: Theory and Experiment*; Springer-Verlag: Berlin, 1999.
- (56) Christanti, Y.; Walker, L. M. Surface tension driven jet break up of strain-hardening polymer solutions. *J. Non-Newtonian Fluid Mech.* **2001**, *100*, 9–26.
- (57) Christanti, Y.; Walker, L. M. Effect of fluid relaxation time of dilute polymer solutions on jet breakup due to a forced disturbance. *J. Rheol.* **2002**, *46*, 733–748.
- (58) Tirtaatmadja, V.; McKinley, G. H.; Cooper-White, J. J. Drop formation and breakup of low viscosity elastic fluids: Effects of molecular weight and concentration. *Phys. Fluids* **2006**, *18*, No. 043101.
- (59) Clasen, C.; Plog, J. P.; Kulicke, W. M.; Owens, M.; Macosko, C.; Scriven, L. E.; Verani, M.; McKinley, G. H. How dilute are dilute solutions in extensional flows? *J. Rheol.* **2006**, *50*, 849–881.
- (60) Erni, P.; Varagnat, M.; Clasen, C.; Crest, J.; McKinley, G. H. Microrheometry of sub-nanolitre biopolymer samples: non-Newtonian flow phenomena of carnivorous plant mucilage. *Soft Matter* **2011**, *7*, 10889–10898.
- (61) Plog, J. P.; Kulicke, W. M.; Clasen, C. Influence of the molar mass distribution on the elongational behaviour of polymer solutions in capillary breakup. *Appl. Rheol.* **2005**, *15*, 28–37.
- (62) Arnolds, O.; Buggisch, H.; Sachsenheimer, D.; Willenbacher, N. Capillary breakup extensional rheometry (CaBER) on semi-dilute and concentrated polyethyleneoxide (PEO) solutions. *Rheol. Acta* **2010**, *49*, 1207–1217.
- (63) Dinic, J.; Biagioli, M.; Sharma, V. Pinch-off dynamics and extensional relaxation times of intrinsically semi-dilute polymer solutions characterized by dripping-onto-substrate rheometry. *J. Polym. Sci., Part B: Polym. Phys.* **2017**, *55*, 1692–1704.
- (64) Dinic, J.; Sharma, V. Macromolecular relaxation, strain, and extensibility determine elastocapillary thinning and extensional

viscosity of polymer solutions. *Proc. Natl. Acad. Sci. U.S.A.* **2019**, *116*, 8766–8774.

(65) Dinic, J.; Sharma, V. Power laws dominate shear and extensional rheology response and capillarity-driven pinching dynamics of entangled hydroxyethyl cellulose (HEC) solutions. *Macromolecules* **2020**, *53*, 3424–3437.

(66) Dinic, J.; Sharma, V. Flexibility, extensibility, and ratio of Kuhn length to packing length govern the pinching dynamics, coil-stretch transition, and rheology of polymer solutions. *Macromolecules* **2020**, *53*, 4821–4835.

(67) Jimenez, L. N.; Dinic, J.; Parsi, N.; Sharma, V. Extensional relaxation time, pinch-off dynamics and printability of semi-dilute polyelectrolyte solutions. *Macromolecules* **2018**, *51*, 5191–5208.

(68) Jimenez, L. N.; Martínez Narváez, C. D. V.; Sharma, V. Capillary breakup and extensional rheology response of food thickener cellulose gum (NaCMC) in salt-free and excess salt solutions. *Phys. Fluids* **2020**, *32*, No. 012113.

(69) Matsumiya, Y.; Watanabe, H. Non-Universal features in uniaxially extensional rheology of linear polymer melts and concentrated solutions: A review. *Prog. Polym. Sci.* **2020**, No. 101325.

(70) Martínez Narváez, C. D. V.; Mazur, T.; Sharma, V. Dynamics and extensional rheology of polymer-surfactant association complexes. *Soft Matter* **2021**, *17*, 6116–6126.

(71) Martínez Narváez, C. D. V.; Dinic, J.; Lu, X.; Wang, C.; Rock, R.; Sun, H.; Sharma, V. Rheology and pinching dynamics of associative polysaccharide solutions. *Macromolecules* **2021**, *54*, 6372–6388.

(72) Lee, K. H.; Kim, H. Y.; Bang, H. J.; Jung, Y. H.; Lee, S. G. The change of bead morphology formed on electrospun polystyrene fibers. *Polymer* **2003**, *44*, 4029–4034.

(73) Huan, S.; Liu, G.; Han, G.; Cheng, W.; Fu, Z.; Wu, Q.; Wang, Q. Effect of experimental parameters on morphological, mechanical and hydrophobic properties of electrospun polystyrene fibers. *Materials* **2015**, *8*, 2718–2734.

(74) Casper, C. L.; Stephens, J. S.; Tassi, N. G.; Chase, D. B.; Rabolt, J. F. Controlling surface morphology of electrospun polystyrene fibers: effect of humidity and molecular weight in the electrospinning process. *Macromolecules* **2004**, *37*, 573–578.

(75) Pai, C.-L.; Boyce, M. C.; Rutledge, G. C. Morphology of porous and wrinkled fibers of polystyrene electrospun from dimethylformamide. *Macromolecules* **2009**, *42*, 2102–2114.

(76) Richard-Lacroix, M.; Pellerin, C. Partial disentanglement in continuous polystyrene electrospun fibers. *Macromolecules* **2015**, *48*, 37–42.

(77) Lin, J.; Shang, Y.; Ding, B.; Yang, J.; Yu, J.; Al-Deyab, S. S. Nanoporous polystyrene fibers for oil spill cleanup. *Mar. Pollut. Bull.* **2012**, *64*, 347–352.

(78) Lee, M. W.; An, S.; Lathe, S. S.; Lee, C.; Hong, S.; Yoon, S. S. Electrospun polystyrene nanofiber membrane with superhydrophobicity and superoleophilicity for selective separation of water and low viscous oil. *ACS Appl. Mater. Interfaces* **2013**, *5*, 10597–10604.

(79) Isik, T.; Demir, M. M. Tailored electrospun fibers from waste polystyrene for high oil adsorption. *Sustainable Mater. Technol.* **2018**, *18*, No. e00084.

(80) Chen, P.-Y.; Tung, S.-H. One-step electrospinning to produce nonsolvent-induced macroporous fibers with ultrahigh oil adsorption capability. *Macromolecules* **2017**, *50*, 2528–2534.

(81) Doan, H. N.; Nguyen, D. K.; Vo, P. P.; Hayashi, K.; Kinashi, K.; Sakai, W.; Tsutsumi, N.; Huynh, D. P. Facile and scalable fabrication of porous polystyrene fibers for oil removal by centrifugal spinning. *ACS Omega* **2019**, *4*, 15992–16000.

(82) Alnaqbi, M. A.; Greish, Y. E.; Mohsin, M. A.; Elumalai, E. J.; Al Blooshi, A. Morphological variations of micro-nanofibrous sorbents prepared by electrospinning and their effects on the sorption of crude oil. *J. Environ. Chem. Eng.* **2016**, *4*, 1850–1861.

(83) Grubbs, R. B.; Grubbs, R. H. 50th anniversary perspective: Living polymerization — emphasizing the molecule in macromolecules. *Macromolecules* **2017**, *50*, 6979–6997.

(84) Walsh, D. J.; Schinski, D. A.; Schneider, R. A.; Guironnet, D. General route to design polymer molecular weight distributions through flow chemistry. *Nat. Commun.* **2020**, *11*, No. 3094.

(85) Dealy, J. M.; Read, D. J.; Larson, R. G. *Structure and Rheology of Molten Polymers: from Structure to Flow Behavior and Back Again*; Carl Hanser Verlag GmbH Co KG, 2018.

(86) Desai, P. S.; Larson, R. G. Constitutive model that shows extension thickening for entangled solutions and extension thinning for melts. *J. Rheol.* **2014**, *58*, 255–279.

(87) James, D. F.; Walters, K. A. Critical Appraisal of Available Methods for the Measurement of Extensional Properties of Mobile Systems. In *Techniques of Rheological Measurement*; Collyer, A. A., Ed.; Elsevier: New York, 1994; pp 33–53.

(88) Li, X.; Ding, B.; Lin, J.; Yu, J.; Sun, G. Enhanced mechanical properties of superhydrophobic microfibrillar polystyrene mats via polyamide 6 nanofibers. *J. Phys. Chem. C* **2009**, *113*, 20452–20457.

(89) Lin, J.; Ding, B.; Yang, J.; Yu, J.; Sun, G. Subtle regulation of the micro- and nanostructures of electrospun polystyrene fibers and their application in oil absorption. *Nanoscale* **2012**, *4*, 176–182.

(90) Singh, V.; Kendall, R. J.; Hake, K.; Ramkumar, S. Crude oil sorption by raw cotton. *Ind. Eng. Chem. Res.* **2013**, *52*, 6277–6281.

(91) Ge, J.; Zhao, H. Y.; Zhu, H. W.; Huang, J.; Shi, L. A.; Yu, S. H. Advanced sorbents for oil-spill cleanup: recent advances and future perspectives. *Adv. Mater.* **2016**, *28*, 10459–10490.

(92) Megelski, S.; Stephens, J. S.; Chase, D. B.; Rabolt, J. F. Micro- and nanostructured surface morphology on electrospun polymer fibers. *Macromolecules* **2002**, *35*, 8456–8466.

(93) Fashandi, H.; Karimi, M. Pore formation in polystyrene fiber by superimposing temperature and relative humidity of electrospinning atmosphere. *Polymer* **2012**, *53*, 5832–5849.

(94) Srinivasarao, M.; Collings, D.; Philips, A.; Patel, S. Three-dimensionally ordered array of air bubbles in a polymer film. *Science* **2001**, *292*, 79–83.

(95) Sharma, V. Colloidal Gold Nanorods, Iridescent Beetles and Breath Figure Templated Assembly of Ordered Array of Pores in Polymer Films. Ph. D. Thesis, Georgia Institute of Technology: Atlanta, GA, 2008.

(96) Sharma, V.; Song, L.; Jones, R. L.; Barrow, M. S.; Williams, P. R.; Srinivasarao, M. Effect of solvent choice on breath-figure-templated assembly of “holey” polymer films. *EPL* **2010**, *91*, No. 38001.

(97) Song, L.; Sharma, V.; Park, J. O.; Srinivasarao, M. Characterization of ordered array of micropores in a polymer film. *Soft Matter* **2011**, *7*, 1890–1896.

(98) Doi, M.; Edwards, S. F. *The Theory of Polymer Dynamics*; Oxford University Press: New York, 1986; p 406.

(99) de Gennes, P.-G. *Scaling Concepts in Polymer Physics*; Cornell University Press: Ithaca, 1979.

(100) Rubinstein, M.; Colby, R. H. *Polymer Physics*; Oxford University Press: New York: 2003.

(101) Prakash, J. R. Universal dynamics of dilute and semidilute solutions of flexible linear polymers. *Curr. Opin. Colloid Interface Sci.* **2019**, *43*, 63–79.

(102) Colby, R. H. Structure and linear viscoelasticity of flexible polymer solutions: comparison of polyelectrolyte and neutral polymer solutions. *Rheol. Acta* **2010**, *49*, 425–442.

(103) Boger, D. V. Highly elastic constant viscosity fluid. *J. Non-Newtonian Fluid Mech.* **1977/1978**, *3*, 87–91.

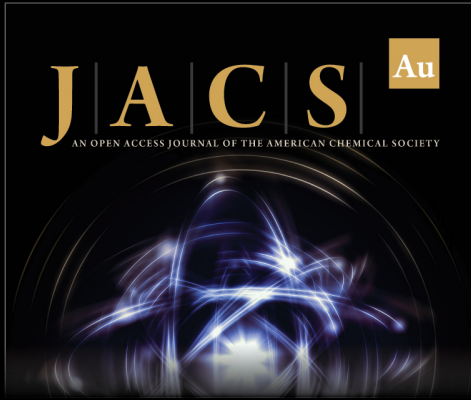
(104) Binnington, R. J.; Boger, D. V. Remarks on non-shear thinning elastic fluids. *Polym. Eng. Sci.* **1986**, *26*, 133–138.

(105) James, D. F. Boger fluids. *Annu. Rev. Fluid Mech.* **2009**, *41*, 129–142.

(106) Middleman, S. Stability of a viscoelastic jet. *Chem. Eng. Sci.* **1965**, *20*, 1037–1040.

(107) Clasen, C.; Eggers, J.; Fontelos, M. A.; Li, J.; McKinley, G. H. The beads-on-string structure of viscoelastic threads. *J. Fluid Mech.* **2006**, *556*, 283–308.

- (108) Ardekani, A.; Sharma, V.; McKinley, G. H. Dynamics of bead formation, filament thinning and breakup of weakly viscoelastic jets. *J. Fluid Mech.* **2010**, *665*, 46–56.
- (109) Sharma, V.; Haward, S. J.; Serdy, J.; Keshavarz, B.; Soderlund, A.; Threlfall-Holmes, P.; McKinley, G. H. The rheology of aqueous solutions of Ethyl Hydroxy-Ethyl Cellulose (EHEC) and its hydrophobically modified Analogue (hmEHEC): Extensional flow response in capillary break-up, jetting (ROJER) and in a cross-slot extensional rheometer. *Soft Matter* **2015**, *11*, 3251–3270.
- (110) Greiciunas, E.; Wong, J.; Gorbatenko, L.; Hall, J.; Wilson, M. C. T.; Kapur, N.; Harlen, O. G.; Vaddillo, D.; Threlfall-Holmes, P. Design and operation of a Rayleigh Ohnesorge jetting extensional rheometer (ROJER) to study extensional properties of low viscosity polymer solutions. *J. Rheol.* **2017**, *61*, 467–476.
- (111) Mathues, W.; Formenti, S.; McLroy, C.; Harlen, O. G.; Clasen, C. CaBER vs ROJER-Different time scales for the thinning of a weakly elastic jet. *J. Rheol.* **2018**, *62*, 1135–1153.
- (112) Sharma, V.; Ardekani, A. M.; McKinley, G. H. In “Beads on a String” Structures and Extensional Rheometry Using jet Break-up, 5th Pacific Rim Conference on Rheology (PRCR-5), 2010.
- (113) Kroesser, F. W.; Middleman, S. Viscoelastic jet stability. *AIChE J.* **1969**, *15*, 383–386.
- (114) Bousfield, D. W.; Keunings, R.; Marrucci, G.; Denn, M. M. Nonlinear analysis of the surface tension driven breakup of viscoelastic filaments. *J. Non-Newtonian Fluid Mech.* **1986**, *21*, 79–97.
- (115) Yarin, A. L. *Free Liquid Jets and Films: Hydrodynamics and Rheology*; Longman Scientific & Technical, 1993.
- (116) Brenn, G.; Liu, Z. B.; Durst, F. Linear analysis of the temporal instability of axisymmetrical non-Newtonian liquid jets. *Int. J. Multiphase Flow* **2000**, *26*, 1621–1644.
- (117) Entov, V. M.; Yarin, A. L. Influence of elastic stresses on the capillary breakup of jets of dilute polymer solutions. *Fluid Dynamics* **1984**, *19*, 21–29.
- (118) Mun, R. P.; Byars, J. A.; Boger, D. V. The effects of polymer concentration and molecular weight on the breakup of laminar capillary jets. *J. Non-Newtonian Fluid Mech.* **1998**, *74*, 285–297.
- (119) Goren, S. L.; Gottlieb, M. Surface-tension-driven breakup of viscoelastic liquid threads. *J. Fluid Mech.* **1982**, *120*, 245–266.
- (120) Bazilevskii, A. V.; Entov, V. M.; Rozhkov, A. N. Elastic stresses in capillary jets of dilute polymer solutions. *Fluid Dyn.* **1985**, *20*, 169–175.
- (121) Rozhkov, A. N. Dynamics and breakup of viscoelastic liquids (A review). *Fluid Dyn.* **2005**, *40*, 835–853.
- (122) Entov, V. M.; Hinch, E. J. Effect of a spectrum of relaxation times on the capillary thinning of a filament of elastic liquid. *J. Non-Newtonian Fluid Mech.* **1997**, *72*, 31–54.
- (123) Yaoita, T.; Isaki, T.; Masubuchi, Y.; Watanabe, H.; Ianniruberto, G.; Marrucci, G. Primitive chain network simulation of elongational flows of entangled linear chains: Role of finite chain extensibility. *Macromolecules* **2011**, *44*, 9675–9682.
- (124) Yaoita, T.; Isaki, T.; Masubuchi, Y.; Watanabe, H.; Ianniruberto, G.; Marrucci, G. Primitive chain network simulation of elongational flows of entangled linear chains: stretch/orientation-induced reduction of monomeric friction. *Macromolecules* **2012**, *45*, 2773–2782.
- (125) Wingstrand, S. L.; Alvarez, N. J.; Huang, Q.; Hassager, O. Linear and nonlinear universality in the rheology of polymer melts and solutions. *Phys. Rev. Lett.* **2015**, *115*, No. 078302.
- (126) Costanzo, S.; Huang, Q.; Ianniruberto, G.; Marrucci, G.; Hassager, O.; Vlassopoulos, D. Shear and extensional rheology of polystyrene melts and solutions with the same number of entanglements. *Macromolecules* **2016**, *49*, 3925–3935.
- (127) Huang, Q.; Hengeller, L.; Alvarez, N. J.; Hassager, O. Bridging the gap between polymer melts and solutions in extensional rheology. *Macromolecules* **2015**, *48*, 4158–4163.
- (128) Huang, Q.; Mednova, O.; Rasmussen, H. K.; Alvarez, N. J.; Skov, A. L.; Almdal, K.; Hassager, O. Concentrated polymer solutions are different from melts: Role of entanglement molecular weight. *Macromolecules* **2013**, *46*, 5026–5035.
- (129) Gupta, R. K.; Nguyen, D. A.; Sridhar, T. Extensional viscosity of dilute polystyrene solutions: Effect of concentration and molecular weight. *Phys. Fluids* **2000**, *12*, 1296–1318.
- (130) Dinic, J.; Zhang, Y.; Jimenez, L. N.; Sharma, V. Extensional relaxation times of dilute, aqueous polymer solutions. *ACS Macro Lett* **2015**, *4*, 804–808.
- (131) Pakravan, M.; Heuzey, M.-C.; Ajji, A. A fundamental study of chitosan/PEO electrospinning. *Polymer* **2011**, *52*, 4813–4824.
- (132) Wang, C.; Fang, C.-Y.; Wang, C.-Y. Electrospun poly (butylene terephthalate) fibers: Entanglement density effect on fiber diameter and fiber nucleating ability towards isotactic polypropylene. *Polymer* **2015**, *72*, 21–29.
- (133) André, A.; Shahid, T.; Oosterlinck, F.; Clasen, C.; Van Ruymbeke, E. Investigating the transition between polymer melts and solutions in nonlinear elongational flow. *Macromolecules* **2021**, *54*, 2797–2810.
- (134) Sridhar, T. An overview of the project M1. *J. Non-Newtonian Fluid Mech.* **1990**, *35*, 85–92.
- (135) McKinley, G. H.; Sridhar, T. Filament-stretching rheometry of complex fluids. *Annu. Rev. Fluid Mech.* **2002**, *34*, 375–415.
- (136) Turan, D.; Gibis, M.; Gunes, G.; Baier, S. K.; Weiss, J. The impact of the molecular weight of dextran on formation of whey protein isolate (WPI)-dextran conjugates in fibers produced by needleless electrospinning after annealing. *Food Funct.* **2018**, *9*, 2193–2200.
- (137) Mirtič, J.; Balažic, H.; Zupančič, Š.; Kristl, J. Effect of solution composition variables on electrospun alginate nanofibers: Response surface analysis. *Polymers* **2019**, *11*, No. 692.
- (138) Rieger, K. A.; Birch, N. P.; Schiffman, J. D. Electrospinning chitosan/poly (ethylene oxide) solutions with essential oils: Correlating solution rheology to nanofiber formation. *Carbohydr. Polym.* **2016**, *139*, 131–138.



JACS Au
AN OPEN ACCESS JOURNAL OF THE AMERICAN CHEMICAL SOCIETY

Editor-in-Chief
Prof. Christopher W. Jones
Georgia Institute of Technology, USA

Open for Submissions

pubs.acs.org/jacsau

ACS Publications
Most Trusted. Most Cited. Most Read.